BIOCHEMISTRY
including biophysical chemistry & molecular biology

Article

pubs.acs.org/biochemistry

Molecular Insight into the Effect of Lipid Bilayer Environments on Thrombospondin-1 and Calreticulin Interactions

Lingyun Wang,[†] Joanne E. Murphy-Ullrich,[‡] and Yuhua Song*[,†]

[†]Department of Biomedical Engineering and [‡]Department of Pathology, The University of Alabama at Birmingham, Birmingham, Alabama 35294, United States

Supporting Information

ABSTRACT: Thrombospondin-1 (TSP1) binding to cell surface calreticulin (CRT) stimulates the association of CRT with low-density lipoprotein (LDL) receptor-related protein (LRP1) to signal focal adhesion disassembly and engagement of cellular activities. A recent study demonstrated that membrane rafts are necessary for TSP1-mediated focal adhesion disassembly, but the molecular role of membrane rafts in mediating TSP1−CRT−LRP1 signaling is unknown. In this study, we investigated the effect of lipid bilayer environments on TSP1 and CRT interactions via atomically detailed molecular dynamics simulations. Results showed that the microscopic structural properties of lipid molecules and mesoscopic mechanical properties and electrostatic potential of the bilayer were significantly different between a 1-palmitoyl-2-oleoyl-*sn*-glycero-3-phosphocholine (POPC) bilayer and a raftlike lipid bilayer [a POPC/cholesterol (CHOL) raftlike lipid bilayer or a POPC/CHOL/sphingomyelin (SM) raftlike lipid bilayer], and the difference was enhanced by SM lipids in a raftlike lipid bilayer. These bilayer property differences affect the interactions of CRT with the bilayer, further influencing CRT conformation and TSP1−CRT interactions. A raftlike lipid bilayer stabilized CRT conformation as compared to a POPC bilayer environment. TSP1 binding to CRT resulted in a conformation for the CRT N-domain more "open" than that of the CRT P-domain in a raftlike lipid bilayer environment, which could facilitate binding of CRT to LRP1 to engage downstream signaling. The open conformational changes of CRT by binding to TSP1 in a raftlike lipid bilayer were enhanced by SM lipids in a lipid bilayer. The direct interactions of both the N- and P-domains of CRT with the bilayer contribute to the more open conformation of CRT in the TSP1−CRT complex on a raftlike lipid bilayer as compared to that on a POPC bilayer. The interactions of CRT or the TSP1−CRT complex with the lipid bilayer also caused CHOL molecules and/or lipids to be more coordinated and to aggregate into patchlike regions in the raftlike lipid bilayers. The lipid and CHOL molecule coordination and aggregation could in turn affect the interactions of CRT with the membrane raft, thereby altering TSP1−CRT interactions and CRT conformational changes that potentially regulate its interactions with LRP1. This study provides molecular insights into the role of lipid bilayer environments in TSP1−CRT interactions and in the CRT conformational changes that are predicted to facilitate binding of CRT to LRP1 to engage downstream signaling events.

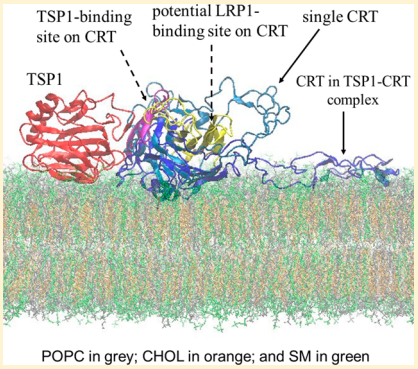

Well-coordinated integration of complex biological and molecular events associated with cell adhesion, cell migration, and extracellular matrix remodeling is required for regenerative medicine, including wound healing in response to injury.[1] Regulation of these cellular processes represents points of intervention for therapeutics for deficient wound healing or excessive repair resulting in fibrosis and scarring.[2−10] The matricellular protein thrombospondin-1 (TSP1) interacts with cell surface protein calreticulin (CRT) to promote binding of CRT to low-density lipoprotein (LDL) receptor-related protein (LRP1) to form the TSP1−CRT−LRP1 ternary complex, which is critical for signaling intermediate adhesion, cell migration, and anoikis resistance.[10−15] TSP1 stimulates collagen expression and matrix deposition by fibroblasts *in vitro* and during tissue remodeling *in vivo* in a CRT-dependent and TGF-β-independent manner.[9] TSP1−CRT interactions also regulate T cell motility and migration.[16,17]

TSP1 is a multifunctional matricellular protein that is widely expressed and secreted from a variety of cell types relevant to wound healing and injury, including fibroblasts, endothelial cells, macrophages, vascular smooth muscle cells, and T lymphocytes.[16−32] Structurally, TSP1 is a large homotrimeric glycoprotein, and each monomer of TSP1 is composed of N- and C-terminal globular domains, which are connected by a rodlike segment.[28] Binding of the N-terminal domain of TSP1 to the cell surface protein CRT enhances the interaction between CRT and LRP1 to form a receptor co-complex that induces intermediate adhesion and stimulates cell migration, anoikis resistance, and collagen synthesis in endothelial cells and fibroblasts.[9,10,12−15] The CRT-binding sequence of TSP1 regulates collagen expression and organization during tissue remodeling.[9] The CRT-binding site in TSP1 has been identified as a sequence of 19 amino acids (amino acids 17−

Received: May 29, 2014
Revised: September 15, 2014
Published: September 15, 2014

 © 2014 American Chemical Society

Table 1. Nine Systems for 300 ns MD Simulations

protein bilayer	CRT	TSP1−CRT complex	no protein
POPC	CRT_POPC	TSP−CRT_POPC	POPC
POPC−CHOL	CRT_POPC−CHOL	TSP−CRT_POPC−CHOL	POPC−CHOL
POPC−CHOL−SM	CRT_POPC−CHOL−SM	TSP−CRT_POPC−CHOL−SM	POPC−CHOL−SM

35, ELTGAARKGSGRRLVKGPD), and lysine residues 24 and 32 of TSP1 are critical for binding of TSP1 to CRT to signal focal adhesion disassembly.[33] The crystal structure of the TSP1 N-domain has been determined,[34] providing a basis for structural studies of the interaction of the TSP1 N-domain with CRT.

CRT, a calcium-binding protein, is localized to and has functions in multiple cellular compartments, including the cell surface, the endoplasmic reticulum, and the extracellular matrix.[35−39] CRT in the endoplasmic reticulum regulates intracellular calcium stores and downstream calcium-dependent signaling, including TGF-β-regulated transcription,[40] and acts as a chaperone, whereas CRT at the cell surface regulates cell adhesion, migration, anoikis resistance, and collagen production when bound to TSP1[9,10,13,14,41,42] in addition to modulating clearance of apoptotic cells and enhancement of wound healing.[43] Structurally, CRT has three domains: a globular β-sandwich N-domain, a proline-rich β-hairpin P-domain, and a calcium-binding C-domain.[44] The TSP1-binding site in CRT is an 18-residue sequence (amino acids 19−36, RWIESKHKSDFGKFVLSS), and a cluster of amino acids 24−26 and amino acids 32−34 in the CRT N-domain is critical for binding of CRT to TSP1.[10,14]

Although the importance of TSP1 and CRT interactions for cell functions related to tissue repair and remodeling is clear, the structural and molecular mechanism by which TSP1 engagement of cell surface CRT initiates signaling complex formation with LRP1 remains unclear. Our recent computational studies of TSP1 and CRT interactions in solvent demonstrated that binding of TSP1 to CRT results in a significant conformational change in CRT upon TSP1 binding,[45] and we know that binding of the TSP1 peptide to CRT increases the association of CRT with LRP1 in cell membrane fractions.[12] Our working model posits that the TSP1-induced changes in the CRT N- and P-domain interactions expose the LRP1-binding site in CRT.[45] Experimental studies suggest that interactions of cell surface CRT with the membrane can potentially influence its responses to TSP1 binding and engagement of LRP1, and membrane rafts are necessary for TSP1-mediated focal adhesion disassembly.[11] The roles of CRT−membrane interactions and of lipid bilayer environments in TSP1−CRT interactions and its induced cellular activities have not been investigated.

Membrane rafts are highly ordered membrane subdomains rich in cholesterol (CHOL) and sphingomyelin (SM).[46] Membrane rafts play important roles in cellular functions, including membrane trafficking and signaling.[47] Experimental studies have demonstrated that membrane rafts can affect membrane protein functions[48−50] and provide the required environment for the function of various proteins such as the acylated Src family kinases, glycosylphosphatidylinositol-anchored proteins, and G protein-coupled receptors.[51] Molecular dynamics (MD) simulations have been used to study the effect of the raftlike lipid bilayer on the bilayer properties, including the condensing effect of CHOL on the bilayer.[52,53] Barker et al. showed that membrane rafts are required for TSP1−CRT binding-induced focal adhesion disassembly;[11] however, the molecular role of membrane rafts in mediating signaling through TSP1−CRT interactions remains unknown. In this study, we investigated the interactions of CRT and the TSP1−CRT complex with a lipid bilayer and the raftlike lipid bilayers and their effects on the conformational changes of CRT and TSP1−CRT interactions via atomically detailed MD simulations. Results from this study provide molecular insights into the roles of the raftlike lipid bilayer in TSP1−CRT interactions.

MATERIALS AND METHODS

Molecular Dynamics Simulations. To elucidate the structural basis and molecular mechanisms underlying the effects of the raftlike lipid bilayer on TSP1−CRT interactions, we performed a total of nine 300 ns molecular dynamics (MD) simulations using the GROMACS 4.5.4 MD simulation package[54] (Table 1). Three types of lipid bilayer systems were used in the MD simulations. A lipid bilayer was modeled as a 1-palmitoyl-2-oleoyl-*sn*-glycero-3-phosphocholine (POPC) bilayer with 1152 lipids. We modeled two different raftlike lipid bilayer environments. The first raftlike lipid bilayer was modeled as a bilayer of POPC lipids mixed with cholesterol (CHOL) (POPC−CHOL bilayer) with CHOL constituting 40% of the number of the molecules in the raftlike lipid bilayer.[53,55−57] The second raftlike lipid bilayer contained sphingomyelin (SM) (POPC−CHOL−SM bilayer) in a 3:4:3 ratio of the number of POPC lipids, CHOL molecules, and SM lipids. The membrane raft is enriched in CHOL,[46] and there is 25−50% of CHOL in the plasma membrane of different cells.[53,58] To investigate the effect of a raftlike bilayer environment on TSP1−CRT interactions, the relatively high concentration of 40% CHOL in a raftlike lipid bilayer is chosen as a representative CHOL concentration to mimic the membrane raft environment.[59] The micro- and mesoscopic properties of the POPC bilayer with or without CHOL and/or SM were examined. The effects of the POPC lipid bilayer and the raftlike lipid bilayers on the conformational changes of CRT and the TSP1−CRT complex and on the interactions of the bilayer with proteins were investigated.

The initial structure of a 128-lipid POPC bilayer was obtained from Tieleman's group[60,61] and was equilibrated for 50 ns. A lipid bilayer composed of 1152 POPC lipids was generated by periodic replication of the equilibrated 128-lipid Tieleman's structure to yield a system with lateral dimensions of roughly 18.6 nm × 18.6 nm. A POPC−CHOL bilayer system (80 POPC and 54 cholesterol; ∼40% CHOL in the system) was obtained from Hub's group[62,63] and equilibrated for 50 ns. A 1206-molecule POPC−CHOL bilayer system with lateral dimensions of roughly 15.8 nm × 15.8 nm (the ratio of the number of POPC lipids and CHOL molecules was kept as 3:2) was formed from Hub's equilibrated 134-molecule POPC−CHOL structure. A POPC−CHOL−SM (1:1:1 POPC:CHOL:SM ratio) bilayer system containing 1024 lipid molecules was obtained from Niemelä.[64] Sixteen random POPC lipids and 17 random SM lipids in each leaflet of the 1024-lipid POPC−CHOL−SM bilayer from Niemelä were

dx.doi.org/10.1021/bi500662v | *Biochemistry* 2014, 53, 6309−6322

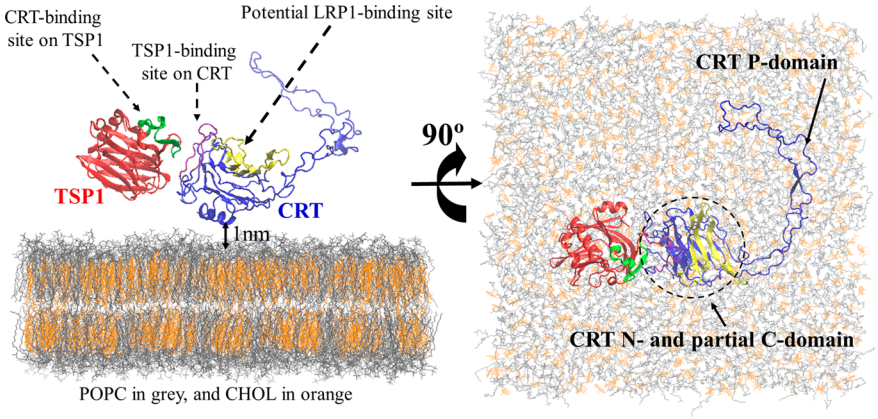

Figure 1. Initial model for the TSP1−CRT complex in a POPC−CHOL raftlike lipid bilayer environment (water and ions are not shown for the sake of clarity) (red for TSP1, blue for CRT, yellow for the potential LRP1-binding site in CRT, green for the CRT-binding site on TSP1, purple for the TSP1-binding site on CRT, gray for the POPC lipid, and orange for CHOL). The left panel is a side view, and the right panel is a top view.

replaced with CHOL to yield a 1024-molecule POPC−CHOL−SM bilayer with a 3:4:3 POPC:CHOL:SM ratio and lateral dimensions of roughly 14.5 nm × 14.5 nm.

A three-dimensional structural model of CRT has been constructed on the basis of the crystal structure of calnexin[65] and the nuclear magnetic resonance (NMR) structure of the P-domain of CRT.[66] This model has been consistent with experimental findings, particularly with respect to the role of His153 in protein folding.[67] In our recent studies,[45] we constructed a TSP1−CRT complex as shown in Figure S1 of the Supporting Information using combined protein docking, MD simulations, and binding free energy calculations, and the constructed complex was validated with the results from biochemical experiments that showed either the K24A and K32A mutations in TSP1 or the mutation of residues 24−26 and 32−34 of CRT to Ala significantly decreased the level of TSP1−CRT complex binding.[10,15,33] With the CRT structure and the TSP1−CRT complex obtained from the previous studies,[45,67] by using VMD,[68] the TSP1−CRT complex is oriented relative to the bilayer surface on the basis of the following considerations. (1) The N-domain of TSP1 used in the simulations is oriented away from the bilayer surface. (2) The potential LRP1-binding site in CRT (yellow region shown in Figure 1) is oriented away from the bilayer surface. (3) Th TSP1-binding site in CRT (purple region shown in Figure 1) and CRT-binding site in TSP1 (green region shown in Figure 1) are oriented away from the bilayer surface. (4) There is at least 0.6 nm between the atoms of the bilayer surface and the atoms of CRT to avoid the steric collision between CRT and the bilayer surface in the initial stages of the simulation. The orientation of the TSP1−CRT complex relative to the surface a POPC lipid bilayer is the same as that of the TSP1−CRT complex relative to the surface of the raftlike lipid bilayers. The orientation of a single CRT relative to the bilayer surface is similar to that of the CRT in the TSP1−CRT complex. The initial model of the TSP1−CRT complex in a POPC−CHOL raftlike lipid bilayer environment is shown in Figure 1 (water and ions are not shown for the sake of clarity) and Figure S2 of the Supporting Information (protein, bilayer, water, and ions are all shown). The distance between the TSP1−CRT complex or CRT and the bilayer boundary along the x and y axes was kept at 1 nm at least to reduce potential artifacts arising from periodicity in MD simulations. We used the Berger's non-polarizable united-atom empirical force field that could properly reproduce the lipid tail order parameters and lipid headgroup area and reasonably reproduce PC lipid headgroup orientation,[64,69,70] GROMOS96 43a2 force field for protein and ions,[71] and single-point charge (SPC) water with Berger's parametrization.[72] These force fields could be found in the GROMACS 4.5.4 MD simulation package.[54]

The MD simulations were performed in a periodic box (the size of the box depends on the simulated system). The MD simulation protocol similar to our previous studies[45,73−80] for the simulated systems includes (1) solvation of the system in a single SPC water box with 100 mM NaCl for the simulated system with a buffer of 2 nm between the protein−bilayer surface and the boundary along the z axis that was ensured to reduce potential artifacts arising from periodicity; (2) steepest descent minimization of the solvent with the protein, lipids, and ions restrained but with mobile water; (3) equilibration of the water with the protein, lipids, and ions restrained at *NPT* at 50 K and 1 atm for 20 ps; (4) warming of the system via a series of 10 ps constant number−volume−temperature MD simulations at 50, 100, 150, 200, 250, 300, and 310 K with LINCS constraints[81] and 2 fs time steps; and (5) a 300 ns equilibration simulation at constant number−pressure−temperature of 310 K and 1 atm using Nose-Hoover temperature coupling[82,83] and Parrinello−Rahman pressure coupling.[84] The final temperature of 310 K was chosen to ensure simulation of the lipid bilayer and raftlike lipid bilayer in the liquid crystalline phase.[59,85] In the production simulations, LINCS constraints[81] were used on all hydrogen−heavy atom bonds to permit a dynamics time step of 2 fs. Electrostatic interactions were calculated by the particle mesh Ewald method (PME)[86,87] with a grid spacing of 0.12 nm and interpolation of order four. The Lennard-Jones cutoffs were set at 1.0 nm.

The lipid headgroup area, autocorrelation of lipid headgroup orientation, and the radius of gyration (R_g) of CRT were calculated over time to ensure that the system reached the steady state during the MD simulations. The lipid headgroup area over time was calculated to evaluate the lipid bilayer equilibration. Lipid headgroup orientation autocorrelation, calculated as in our previous study,[80] was used to examine the autocorrelation function of the time-dependent vector between the phosphorus and nitrogen (PN angle) of the lipid molecule and to determine the dynamical relaxation of lipid molecules. The radius of gyration (R_g) of a single CRT or CRT in the TSP1−CRT complex in different bilayer environments

dx.doi.org/10.1021/bi500662v | *Biochemistry* 2014, 53, 6309−6322

was calculated over time to determine the protein's equilibration tendencies. The simulation trajectories after the initial equilibration and relaxation were used for the analyses of protein conformation, the interactions of protein with the bilayer, and the micro- and mesoscopic properties of the lipid bilayer and the raftlike lipid bilayers.

Statistical Methods. To compare differences in micro- and mesoscopic properties between a POPC lipid bilayer and raftlike lipid bilayers, which could also affect interactions of cell surface CRT with TSP1, the average values and standard deviations of the analyzed variables were calculated. Because the adjacent snapshots from the MD trajectory have the tendency to be correlated with each other, the autocorrelation times[79,88] for the studied variables were obtained to resample the trajectories into statistically independent periods to calculate the standard deviations for studied variables. With the obtained decorrelation times, bootstrap analysis[89] was performed following an analysis protocol similar to that of Chen and Pappu and our previous studies.[45,73−80] Significant differences in the mean and standard deviations for the studied variables were determined using the Student's t test[90] with 95% confidence.

RESULTS AND DISCUSSION

Equilibration of the Simulated Systems. The lipid headgroup areas of POPC lipids in a POPC lipid bilayer and the POPC−CHOL and POPC−CHOL−SM raftlike lipid bilayer over 300 ns MD simulations were calculated to evaluate the equilibration of the bilayer system (Figure S3a of the Supporting Information). The lipid headgroup orientation (the angle between the phosphorus and nitrogen of the lipid molecule) autocorrelations for a POPC lipid bilayer, a POPC−CHOL raftlike lipid bilayer, and a POPC−CHOL−SM raftlike lipid bilayer were calculated to determine the dynamic relaxation of lipid molecules (Figure S3b of the Supporting Information). These calculations showed that all the bilayer systems reached an initial steady state after 200 ns (Figure S3a,b of the Supporting Information). Radii of gyration of CRT showed that the protein reached the initial steady state after 200 ns (Figure S3c of the Supporting Information). On the basis of the results of the lipid headgroup area, lipid headgroup orientation autocorrelations, and the radius of gyration of CRT over 300 ns MD simulations, the last 100 ns MD simulation trajectories were used for the analyses of the effect of the raftlike lipid bilayer on TSP1−CRT interactions.

Microscopic and Mesoscopic Properties of a POPC Lipid Bilayer and Raftlike Lipid Bilayers. We analyzed the micro- and mesoscopic properties of a POPC bilayer and two raftlike lipid bilayers that could affect interactions of CRT with a bilayer, further influencing TSP1−CRT interactions and the conformational status of CRT in different bilayer environments. For microscopic properties, we examined the lipid headgroup area, lipid tail order, and bilayer thickness. For mesoscopic properties, we analyzed the bilayer mechanical behavior-related parameters (bending modulus and compressibility modulus) and analyzed the electrostatic potential of a POPC bilayer and raftlike lipid bilayers.

Microscopic Properties. The headgroup area per lipid molecule was calculated by the projected area that spanned the lateral dimensions of the simulated system divided by the number of lipid molecules. The result showed that the lipid headgroup area in a raftlike lipid bilayer, either a POPC−CHOL raftlike lipid bilayer (0.42 ± 0.001 nm^2) or a POPC−CHOL−SM raftlike lipid bilayer (0.41 ± 0.001 nm^2), was significantly smaller than that in a POPC bilayer (0.60 ± 0.001 nm^2) (Table 2), which was consistent with the observations in previous studies.[64,91] Previous experimental studies show that for a salt-free POPC bilayer, values of 0.66 nm^2 (T = 310 K),[92] 0.68 nm^2 (T = 303.15 K),[93] 0.60 nm^2 (T = 303.15 ± 2 K), 0.65 nm^2 (T = 298 K),[94] and 0.63 nm^2 (T = 297 K)[95] have been reported for the area per lipid for POPC bilayers. Previous studies also show that the addition of NaCl in a POPC bilayer system significantly affects the structural properties of a POPC lipid bilayer through the binding of cations to the lipid−water interface, which decreases the area per lipid for a salt-free POPC bilayer at 310 K from 0.65 to 0.60 nm^2.[91] The lipid headgroup area of 0.60 nm^2 for a POPC lipid bilayer with NaCl at 310 K in this study is consistent with that in a previous study.[91]

Table 2. Structural Properties of a Lipid Bilayer and Two Raftlike Lipid Bilayers

system	A^a (nm^2)	d^b (nm)
POPC bilayer	0.60 ± 0.001	3.99 ± 0.009
POPC−CHOL raftlike lipid bilayer	0.42 ± 0.001	4.54 ± 0.015
POPC−CHOL−SM raftlike lipid bilayer	0.41 ± 0.001	4.53 ± 0.005

[a]Lipid headgroup area. [b]Bilayer thickness.

The thickness of the bilayer was calculated as the distance between the phosphorus atoms of lipids in two leaflets averaged over the last 100 ns simulation trajectories. Results showed that the thickness of a raftlike lipid bilayer, either a POPC−CHOL raftlike lipid bilayer (4.55 ± 0.015 nm) or a POPC−CHOL−SM raftlike lipid bilayer (4.53 ± 0.005 nm), was significantly larger than that of a POPC bilayer (3.99 ± 0.009 nm) (Table 2), indicating the lipids are more ordered in a raftlike lipid bilayer than that in a POPC bilayer. There was no significant difference in lipid headgroup area and bilayer thickness between a POPC−CHOL raftlike lipid bilayer and a POPC−CHOL−SM raftlike lipid bilayer (Table 2).

The tail order parameters of the two acyl chains of POPC lipids were calculated for the comparison of POPC tail order in a POPC bilayer, a POPC−CHOL raftlike lipid bilayer, and a POPC−CHOL−SM raftlike lipid bilayer using the last 100 ns simulation trajectories (Figure 2). The order parameters were calculated using the method described previously.[80,96] Results showed that the tail order of the POPC lipid was significantly increased in a raftlike lipid bilayer compared to that in a POPC bilayer. There was no significant difference in POPC tail order in a POPC−CHOL raftlike lipid bilayer or in a POPC−CHOL−SM raftlike lipid bilayer. These changes, together with the headgroup area per lipid and bilayer thickness presented above, suggest that CHOL and SM molecules in raftlike lipid bilayers cause packing and ordering of the bilayer.

Mesoscopic Properties. Mechanical Properties. Cell membrane mechanical properties could directly affect cellular functions through their permeability and deformability. Studies have shown that the elastic properties of a lipid bilayer influence the function of membrane-bound proteins.[97] To understand the cell surface CRT functions in different bilayer environments, we analyzed the mechanical behavior of a POPC bilayer, a POPC−CHOL raftlike lipid bilayer, and a POPC−CHOL−SM raftlike lipid bilayer. The area compressibility modulus that describes the energetics of increases and decreases in membrane areas was calculated on the basis of

dx.doi.org/10.1021/bi500662v | Biochemistry 2014, 53, 6309−6322

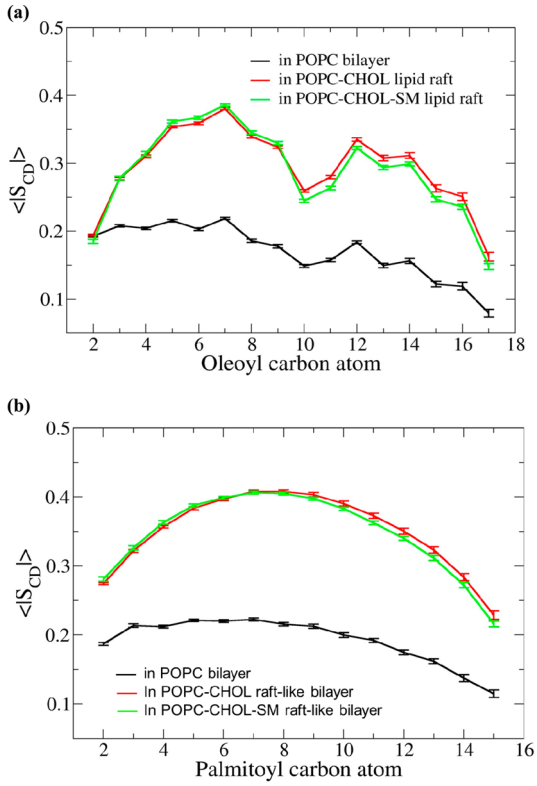

Figure 2. POPC lipid tail order parameter in a POPC bilayer, a POPC−CHOL raftlike lipid bilayer, and a POPC−CHOL−SM raftlike lipid bilayer. (a) Tail order parameter for the oleoyl carbon atom. (b) Tail order parameter for the palmitoyl carbon atom. The error bars are the standard deviation calculated on the basis of the statistically independent periods of MD simulation trajectories obtained as described in Statistical Methods.

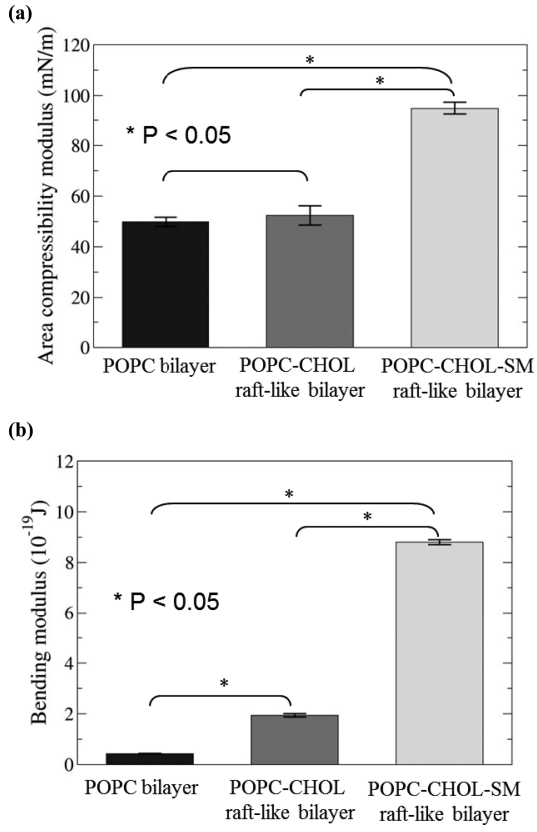

Figure 3. Mechanical properties of a POPC bilayer, a POPC−CHOL raftlike lipid bilayer, and a POPC−CHOL−SM raftlike lipid bilayer: (a) area compressibility modulus and (b) bending modulus. The error bars are the standard deviation calculated on the basis of the statistically independent periods of MD simulation trajectories obtained as described in Statistical Methods. Asterisks denote that the difference is statistically significant on the basis of the mean and standard deviation of the analyzed variable (Student's t test; $p < 0.05$).

the fluctuations of the projected area according to the formula used in previous studies.[80,98] Results showed that although a POPC−CHOL raftlike lipid bilayer increased the area compressibility modulus (52.38 ± 3.79 mN/m) compared to that of a POPC bilayer (49.85 ± 1.82 mN/m), the change was not significant (Figure 3a). With the SM lipids in the raftlike lipid bilayer (a POPC−CHOL−SM raftlike lipid bilayer), the area compressibility modulus was significantly increased to 94.89 ± 2.64 mN/m (Figure 3a).

The bending modulus of a bilayer was calculated on the basis of the total root-mean-square amplitude of the undulation modes in the system and the project area of the system as in previous studies.[80,99] Similar to the area compressibility modulus result, a POPC−CHOL raftlike lipid bilayer slightly increased the bending modulus (1.94×10^{-19} J) compared to that of a POPC bilayer (0.43×10^{-19} J), but for a POPC−CHOL−SM raftlike lipid bilayer, the bending modulus was significantly increased to 8.80×10^{-19} J (Figure 3b). These results indicated that raftlike lipid bilayer integrity is important for interactions of cell surface CRT with the membrane bilayer and CRT functions, consistent with experimental observations.[11]

Electrostatic Potential. The electrostatic potentials of the simulated systems were calculated along the bilayer normal (z axis) from the average charge densities by solving Poisson's equation via an integral of the charge density along the z direction as in the previous study with the available analysis program in the GROMACS 4.5.4 MD simulation package.[54,80] Significantly different electrostatic potentials were observed at the water−bilayer interface for a POPC bilayer, a POPC−CHOL raftlike lipid bilayer, and a POPC−CHOL−SM raftlike lipid bilayer (Figure S4 of the Supporting Information).

The POPC lipid has an unsaturated double bond in the oleoyl chain, which results in a kink in the acyl chain, preventing the POPC lipids from tightly packing to each other.[100] The disordered arrangement of POPC lipids makes the POPC bilayer have a fluid property.[101] SM lipids that exist in membrane rafts have two saturated acyl chains.[46] The CHOL molecule has a planar structure and thus can intercalate between saturated acyl chains of the lipid.[102,103] In this way, CHOL holds the lipids tightly together, which could increase lipid order and membrane rigidity (Figures 2 and 3). The CHOL molecule can also change the physical properties of a lipid bilayer by forming laterally segregated raftlike domains.[104,105] The interactions of the acyl chain of the lipid with CHOL result in a more extended conformation of neighboring hydrocarbon chains, which can increase membrane thickness[106] as shown in Table 2. Both the raftlike POPC−CHOL bilayer and the POPC−CHOL−SM bilayer are thicker than the POPC bilayer (Table 2). In addition, experimental and computational studies indicate that direct interactions between the PC lipid headgroup and CHOL can cause rearrangement of the lipid headgroup,[107,108] which could result in the different electrostatic potentials at the water−bilayer interface for a

dx.doi.org/10.1021/bi500662v | *Biochemistry* 2014, 53, 6309−6322

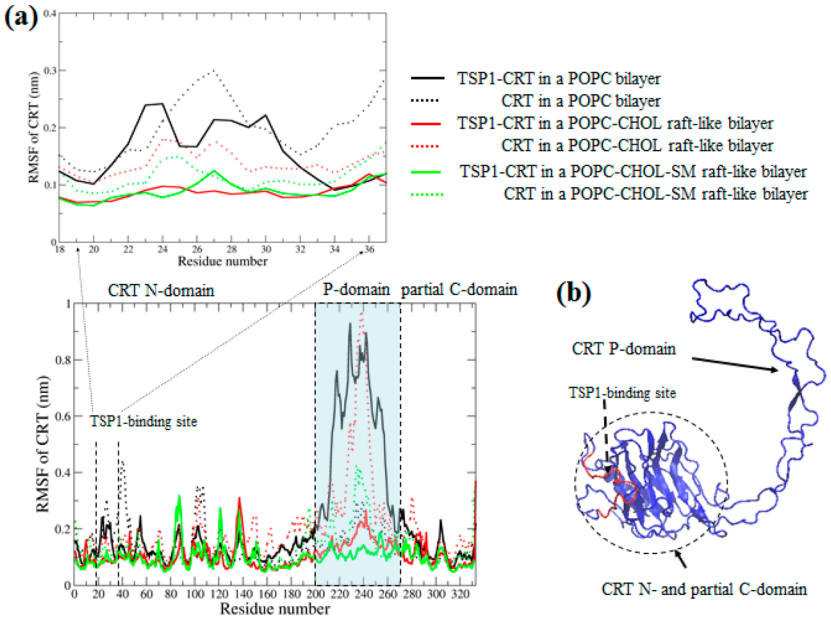

Figure 4. (a) Root-mean-square-fluctuation comparison of CRT (solid black line for CRT in the TSP1−CRT_POPC system, dotted black line for a single CRT in the CRT_POPC system, solid red line for CRT in a TSP1−CRT_POPC−CHOL system, dotted red line for a single CRT in the CRT_POPC−CHOL system, solid green line for CRT in the TSP1−CRT_POPC−CHOL−SM system, and dotted green line for a single CRT in the CRT_POPC−CHOL−SM system). (b) Cartoon of CRT showing the CRT N-domain (residues 1−200) and a partial C-domain (residues 271−327), the CRT P-domain (residues 201−270), and the TSP1-binding site in CRT.

POPC bilayer and raftlike lipid bilayers as observed in Figure S4 of the Supporting Information.

The changes in the microscopic and mesoscopic properties of raftlike lipid bilayers by CHOL and SM could affect interactions of CRT with the bilayer and further affect CRT conformation and TSP1−CRT interactions, thus influencing CRT-mediated signaling in different bilayer environments.

CRT Conformational Changes Induced by Binding to TSP1 and Changes of TSP1−CRT Interactions in Different Bilayer Environments. *Root-Mean-Square Fluctuation (rmsf) of CRT Analyses.* The conformational stability of CRT could directly affect TSP1−CRT binding. We examined the rmsf of CRT. The rmsf of the CRT-binding site for TSP1 was determined from the rmsf of CRT to examine CRT conformational flexibility caused by binding of CRT to TSP1 in different bilayer environments in detail (Figure 4). Results showed that binding of TSP1 to CRT stabilized the TSP1-binding site of CRT regardless of whether binding occurred in a POPC bilayer, in a POPC−CHOL raftlike lipid bilayer, or in a POPC−CHOL−SM raftlike lipid bilayer environment, which was the same as observed in a solvent environment in our previous study.[45] Figure 4 also shows that for the TSP1−CRT complex, the raftlike lipid bilayer, either a POPC−CHOL raftlike lipid bilayer (red solid line) or a POPC−CHOL−SM raftlike lipid bilayer (green solid line), stabilizes the CRT-binding site for TSP1 to a greater extent than the TSP1−CRT complex in a POPC bilayer (black solid line). The stronger stabilization of the conformation of the CRT-binding site for TSP1 by raftlike lipid bilayers compared to that in a POPC bilayer was also observed for CRT alone (dotted red line for a POPC−CHOL raftlike lipid bilayer, green dotted line for a POPC−CHOL−SM raftlike lipid bilayer, and black dotted line for a POPC bilayer). The P-domain of CRT in the TSP1−CRT complex was also stabilized by raftlike lipid bilayers as compared to a POPC bilayer. The raftlike lipid bilayer with SM lipids (a POPC−CHOL−SM raftlike lipid bilayer) enhanced the CRT conformational stabilization as compared to that of a POPC−CHOL raftlike lipid bilayer. The conformational flexibility of the P-domain of a single CRT is also affected by the different bilayer environment. These changes in conformational stability of CRT could directly affect TSP1−CRT interactions and binding of CRT to LRP1.

Radius of Gyration of CRT and the Potential LRP1-Binding Site in CRT. Radius of Gyration of CRT. The radius of gyration (R_g) of a protein could be used to evaluate the size and compactness of a protein structure. A schematic representation of the radius of gyration of a representative structure of CRT alone and CRT in the TSP1−CRT complex in a POPC−CHOL raftlike lipid bilayer environment is shown in Figure 5a. To evaluate the conformation of CRT and CRT in the TSP1−CRT complex in different bilayer environments, the radius of gyration of CRT were calculated over 300 ns MD simulation trajectories (Figure S3c of the Supporting Information), and the mean and deviation of the radius of gyration over the last 100 ns MD trajectories were calculated (Figure 5b). The representative structures for CRT alone and the TSP1−CRT complex shown in Figure 5a were obtained by clustering analysis using MMTSB toolset.[109] Protein Data Bank (PDB) structures for a single CRT and the TSP1−CRT complex were generated from the last 100 ns MD trajectories with a 100 ps interval. A centroid structure was obtained by averaging the PDB structures. Clustering analysis was performed using the K-means algorithm[110] based on the root-mean-square deviation (rmsd) similarity of the structures. The structure that has the lowest rmsd from the centroid structure was obtained as the representative structure.

The R_g results for CRT in the last 100 ns simulations showed that in a POPC bilayer environment, binding of TSP1 to CRT significantly decreased the radius of gyration of CRT as compared to that of a single CRT (Figure 5b), suggesting a tighter globular conformation of CRT in the TSP1−CRT complex. In a raftlike lipid bilayer environment, either the

dx.doi.org/10.1021/bi500662v | *Biochemistry* 2014, 53, 6309−6322

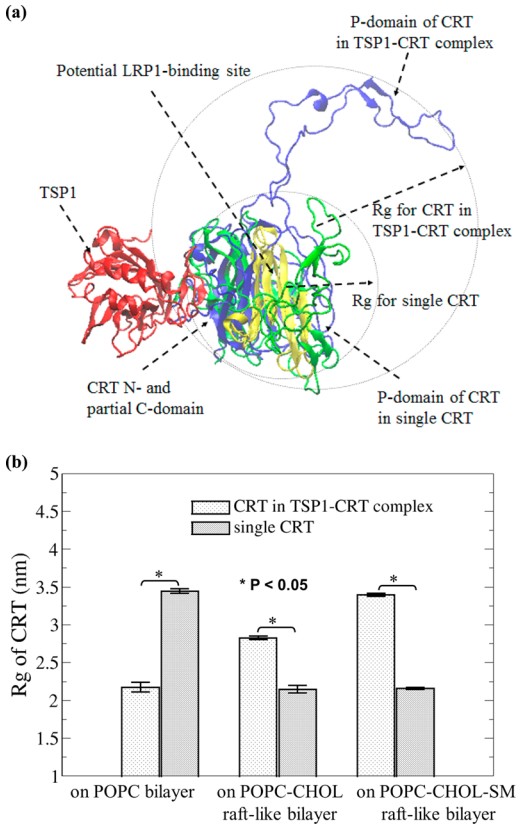

Figure 5. CRT conformation represented by the radius of gyration (R_g). (a) Schematic representation of the radius of gyration and the potential LRP1-binding site in CRT (the bilayer is not shown for the sake of clarity; red for TSP1, blue for CRT in the TSP1−CRT complex, green for a single CRT, and yellow for the potential LRP1-binding site on CRT). (b) Radius of gyration comparison of CRT alone with CRT in the TSP1−CRT complex on a POPC bilayer, a POPC−CHOL raftlike lipid bilayer, and a POPC−CHOL−SM raftlike lipid bilayer. The error bars are the standard deviations calculated on the basis of the statistically independent periods of MD simulation trajectories as described in Statistical Methods. Asterisks denote that the difference is statistically significant on the basis of the mean and standard deviation of the analyzed variable (Student's t test; $p < 0.05$).

POPC−CHOL raftlike lipid bilayer or the POPC−CHOL-SM raftlike lipid bilayer, binding of TSP1 to CRT significantly increased the radius of gyration of CRT compared to that of a single CRT (Figure 5b), suggesting a more "open" conformation of CRT in the TSP1−CRT complex. The overlay of the representative structures of CRT alone and the CRT in the TSP1−CRT complex in a POPC bilayer (Figure S6a of the Supporting Information), a POPC−CHOL raftlike lipid bilayer (Figure S6b of the Supporting Information), and a POPC−CHOL−SM raftlike lipid bilayer (Figure S6c of the Supporting Information) explicitly showed a conformation of CRT in the TSP1−CRT complex more open than that of CRT alone in both the POPC−CHOL and POPC−CHOL−SM raftlike lipid bilayers (Figure S6 of the Supporting Information). The raftlike lipid bilayer with SM lipids (POPC−CHOL−SM raftlike lipid bilayer) supported an enhanced open CRT conformation upon TSP1 binding as compared to that of the TSP1−CRT complex in a POPC−CHOL raftlike lipid bilayer (Figure 5b and Figure S6 of the Supporting Information).

Potential LRP1-Binding Site in CRT. TSP1 interacts with the cell surface CRT to promote binding of CRT to LRP1 to form the TSP1−CRT−LRP1 ternary complex, which is critical for signaling intermediate adhesion, cell migration, and anoikis resistance.[10−15] The binding site in TSP1-bound CRT for LRP1 remains unknown. The complex structure of LRP1 increases the level of difficulty of biochemically identifying the binding site in CRT for LRP1 by trial and error. The combined quantitative conformational analyses of CRT before and after binding to TSP1 from MD simulation with hydropathy analyses for CRT and the ligand binding-type repeat of LRP1[111] provide an alternative approach to complementing biochemical experiments. On the basis of the conformational comparison of CRT alone and CRT in the TSP1−CRT complex in a POPC−CHOL raftlike lipid bilayer environment shown as Figure 5a, and hydropathy analyses and the restriction that the binding region for LRP1 does not overlap the TSP1-binding site in CRT (consistent with the observation that LRP1 does not affect the TSP1−CRT interaction), we proposed that amino acids 96−150 colored yellow in Figure 5a in the CRT N-domain may represent the potential binding site in CRT for LRP1.

The more open conformation of the CRT N-domain (residues 1−200) and the partial C-domain (residues 271−327) relative to the P-domain (residues 201−270) induced by TSP1 binding might expose these residues to permit CRT−LRP1 binding and signaling through the TSP1−CRT−LRP1 complex.[10−15]

Distance Matrix of CRT Analyses. The distance matrix was calculated for the average distance between the residues in CRT and between the residues of CRT in the TSP1−CRT complex on a POPC bilayer (Figure 6a), on a POPC−CHOL raftlike lipid bilayer (Figure 6b), and on a POPC−CHOL−SM raftlike lipid bilayer (Figure 6c) over the last 100 ns of MD simulations. The top right half of each figure in Figure 6 shows the distance matrix for CRT in the TSP1−CRT complex, and the bottom left half shows the distance matrix for CRT alone. Results showed that in a POPC bilayer environment, the distance between the partial CRT P-domain (amino acids 201−270) and the CRT N-domain (amino acids 1−200) for a single CRT is larger than that of CRT in the TSP1−CRT complex (Figure 6a), which was supported by the results for the radius of gyration of CRT shown in Figure 5. This suggested that in a POPC bilayer environment, binding of TSP1 to CRT resulted in a "closed" conformation between the tail-like P-domain of CRT and the globular CRT N-domain. The closed conformation between the CRT N-domain and P-domain could hide residues important for the recruitment of LRP1 to CRT as the predicted potential LRP1-binding site in CRT (yellow region in Figure 5a) to form the TSP1−CRT−LRP1 ternary complex that signals focal adhesion disassembly and resistance to anoikis.[10,12,13] Results also showed that in a raftlike lipid bilayer environment, either the POPC−CHOL bilayer or the POPC−CHOL−SM bilayer, binding of TSP1 to CRT significantly increased the distance between the partial CRT P-domain (amino acids 201−270) and the CRT N-domain (amino acids 1−200), with the POPC−CHOL−SM raftlike lipid bilayer resulting in a greater distance, as shown by the increased degree of the red patch in panels b and c of Figure 6. These observations were supported by results from the radius of gyration of CRT showing that in raftlike lipid bilayer environments, binding of TSP1 to CRT significantly increased the radius of gyration of CRT, which was further enhanced by

dx.doi.org/10.1021/bi500662v | Biochemistry 2014, 53, 6309−6322

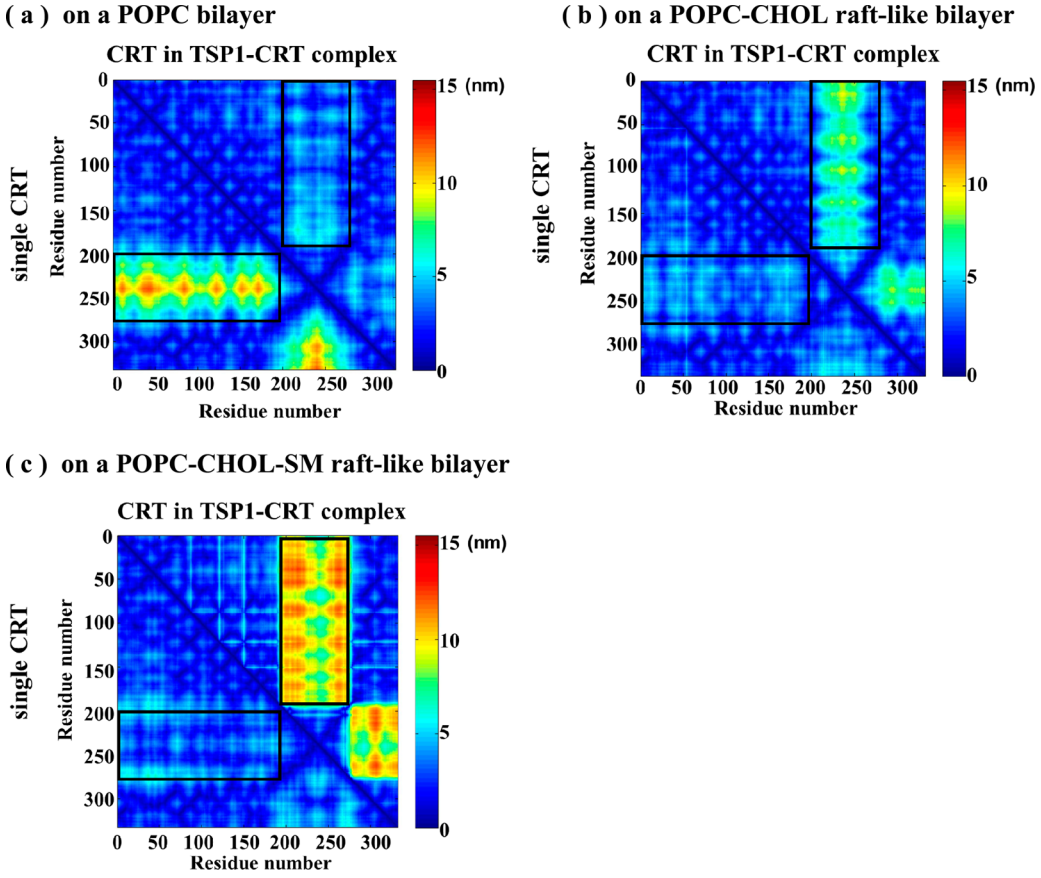

Figure 6. Distance matrix map for the comparison of distances of the residues in CRT alone (bottom left) with CRT in the TSP1−CRT complex (top right) (distances in nanometers) (a) on a POPC bilayer, (b) on a POPC−CHOL raftlike lipid bilayer , and (c) on a POPC−CHOL−SM raftlike lipid bilayer. The black boxes represent distances between the partial CRT P-domain (amino acids 201−270) and the CRT N-domain (amino acids 1−200) (red for longer distances between residues and blue for shorter distances between residues).

the raftlike lipid bilayer with SM lipids (Figure 5b). These results suggest that binding of TSP1 to CRT results in a configuration between the CRT N- and P-domains more open than that of CRT alone in a raftlike lipid bilayer environment. The more open conformation of the CRT N-domain relative to that of the P-domain induced by TSP1 binding might expose additional residues important for recruitment of LRP1 to CRT (yellow region in Figure 5a) to form a ternary signaling complex.

Analyses of Hydrogen Bonds between the TSP1-Binding Site in CRT and the CRT-Binding Site in TSP1. We analyzed the number of hydrogen bonds formed between the TSP1-binding site in CRT and the CRT-binding site in TSP1 on a POPC bilayer, on a POPC−CHOL raftlike lipid bilayer, and on a POPC−CHOL−SM raftlike lipid bilayer (Figure 7). A hydrogen bond was determined when the distance between the hydrogen and acceptor was <3.5 Å and the hydrogen−donor−acceptor angle was >150°. The number of hydrogen bonds between the TSP1-binding site in CRT and the CRT-binding site in TSP1 was calculated by summing all the hydrogen bonds within the regions and was averaged over the production simulations. The results showed that more hydrogen bonds formed between the TSP1-binding site in CRT and the CRT-binding site in TSP1 in raftlike lipid bilayers than in a POPC bilayer (Figure 7).

The results from the root-mean-square fluctuation of CRT (Figure 4), the radius of gyration of CRT (Figure 5), and the distance matrix of CRT (Figure 6) showed that raftlike lipid

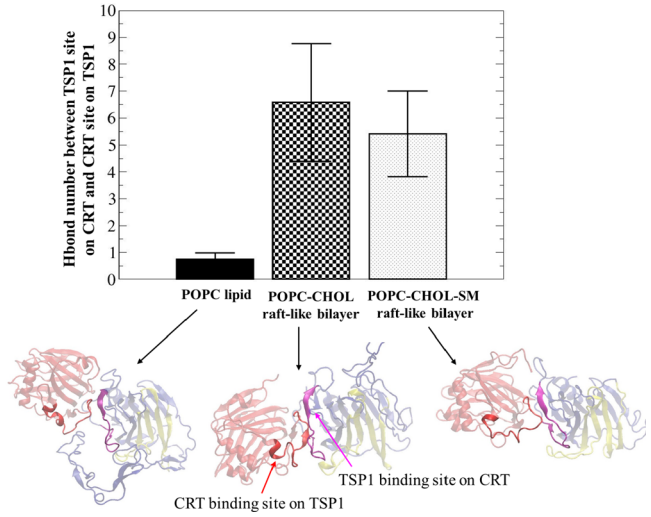

Figure 7. Comparison of the number of hydrogen bonds formed between the TSP1-binding site in CRT and the CRT-binding site in TSP1 on a POPC bilayer, on a POPC−CHOL raftlike lipid bilayer, and on a POPC−CHOL−SM raftlike lipid bilayer. The TSP1-binding site in CRT is colored pink and the CRT-binding site in TSP1 red. The error bars are the standard deviations calculated on the basis of the statistically independent periods of MD simulation trajectories as described in Statistical Methods.

dx.doi.org/10.1021/bi500662v | *Biochemistry* 2014, 53, 6309−6322

bilayers stabilize the CRT conformation, binding of TSP1 to CRT results in a conformation for the CRT N-domain more open than that for the CRT P-domain in a raftlike lipid bilayer environment, and the effects of the raftlike lipid bilayer environment were potentiated by SM lipids. The conformational changes of CRT by binding to TSP1 in different bilayer environments could directly affect TSP1−CRT interactions as observed in the hydrogen bond analyses between the TSP1-binding site in CRT and the CRT-binding site in TSP1 (Figure 7), which shows that more hydrogen bonds formed between the TSP1-binding site in CRT and the CRT-binding site in TSP1 in raftlike lipid bilayers than in a POPC bilayer. These observations provide structural and molecular insights into the role of the bilayer environments in TSP1−CRT interactions and the induced CRT conformational changes, which are proposed to affect binding of CRT to LRP1 and signaling.[10−15]

Interactions between CRT and a Lipid Bilayer or Raftlike Lipid Bilayer. We examined the interactions between CRT and a POPC lipid bilayer or a raftlike lipid bilayer to improve our understanding of the effect of different bilayer environments on TSP1−CRT interactions and on the conformational changes of CRT bound to TSP1. We also examined the effect of protein on the coordination and/or aggregation among the POPC lipid, CHOL molecule, and SM lipid in the raftlike lipid bilayers.

Analyses of the Interactions of CRT with a Lipid Bilayer or Raftlike Lipid Bilayer. Figure 8 illustrates the mass density of

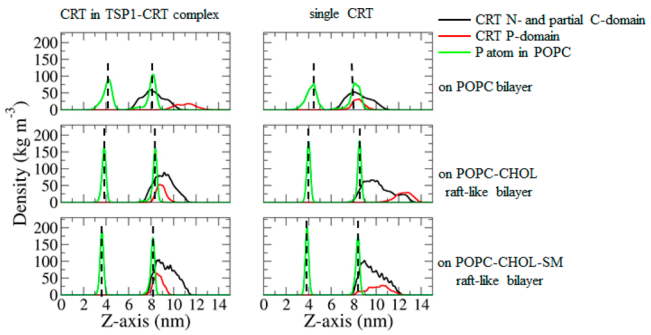

Figure 8. Comparison of the mass density of CRT as a function of distance along the bilayer normal (z axis) on a POPC bilayer, on a POPC−CHOL raftlike lipid bilayer, and on a POPC−CHOL−SM raftlike lipid bilayer. The dotted lines are the mass density peaks of the phosphorus atoms of POPC lipids, indicating the surfaces of the bilayer.

CRT or CRT in the TSP1−CRT complex as a function of distance along the bilayer normal (z axis) in different bilayer environments, showing the position of CRT relative to the bilayer. The dotted lines in Figure 8 are the mass density peaks of the phosphorus (P) atom of POPC lipids, indicating the surfaces of the bilayer. Results showed that in a POPC bilayer environment, for CRT alone, the CRT N-domain, partial C-domain, and P-domain were mainly located at a position similar to those of the P atoms of POPC lipids (water−bilayer interface), and for CRT in the TSP1−CRT complex, only the CRT N-domain and the partial C-domain were mainly positioned at the water−bilayer interface and the CRT P-domain was oriented away from the bilayer surface. In a raftlike lipid bilayer environment, either the POPC−CHOL raftlike lipid bilayer or the POPC−CHOL−SM raftlike lipid bilayer, the N-domain and partial C-domain and P-domain of CRT in the TSP1−CRT complex were located at a position similar to that of the P atom of POPC lipid (water−bilayer surface). For CRT alone in a raftlike lipid bilayer environment, although the N-domain and partial C-domain of CRT were mainly positioned above the P atom of POPC lipid (water−bilayer interface), the P-domain of CRT was oriented away from the bilayer surface. The results showed that the N-domain and partial C-domain and P-domain of CRT in the TSP1−CRT complex on a membrane raft directly interacted with lipid headgroups in contrast to CRT in the TSP1−CRT complex on a POPC bilayer in which only the CRT N-domain and partial C-domain directly interacted with lipid headgroups. The results indicated that the direct interactions of both the N-domain and the partial C-domain and P-domain of CRT, particularly the P-domain of CRT with lipid headgroups, could contribute to the more open conformation of CRT in the TSP1−CRT complex on a raftlike lipid bilayer compared to that on a POPC bilayer as observed in Figures 5 and 6 and Figure S5 of the Supporting Information.

To further examine the interactions of the N-domain and partial C-domain and P-domain of CRT in the TSP1−CRT complex with a lipid bilayer, radial distribution functions (RDFs) of the N-domain and partial C-domain and P-domain of CRT in the TSP1−CRT complex with the phosphorus atoms of the POPC lipid headgroup, the cholesterol hydroxyl oxygens, and the phosphorus atoms of the SM lipid headgroup on a POPC bilayer, on a POPC−CHOL raftlike lipid bilayer, and on a POPC−CHOL−SM raftlike lipid bilayer were calculated and are shown in panels a and b of Figure 9. The RDF results show that in a POPC bilayer, the CRT N-domain and partial C-domain strongly coordinate with the POPC lipids, but the CRT P-domain does not have coordination with the POPC lipids. In a POPC−CHOL raftlike bilayer, both the CRT N-domain and the partial C-domain and P-domain strongly coordinate with the POPC lipids and weakly coordinated with CHOL, but the coordination of the POPC lipid and CHOL with the CRT P-domain is stronger than that of the CRT N-domain and the partial C-domain. In a POPC−CHOL−SM raftlike bilayer, the coordination of the POPC lipid with the CRT P-domain is much stronger than that with the CRT N-domain and partial C-domain, although both the CRT N-domain and the partial C-domain and P-domain strongly coordinate with the SM lipids and weakly coordinated with CHOL, and the coordination of the SM lipid and CHOL with the CRT P-domain is stronger than that with the CRT N-domain and the partial C-domain (Figure 9a,b). The snapshots from the MD trajectories depicting the coordination of the N-domain and the partial C-domain and P-domain of CRT in the TSP1−CRT complex with the POPC lipids in a POPC bilayer (Figure 9c), with POPC lipids and CHOL molecules in a POPC−CHOL raftlike lipid bilayer (Figure 9d), and with POPC lipids, CHOL molecules, and SM lipids in a POPC−CHOL−SM raftlike lipid bilayer (Figure 9e) are shown in Figure 9. The lipids and CHOL molecules whose atoms are within 3.5 Å of CRT are shown together with CRT in Figure 9c−e. The residues in the N-domain and the partial C-domain and P-domain of CRT in the TSP1−CRT complex that interacted with the bilayer are listed in Table S1 of the Supporting Information. These results showed that the coordination of the CRT N-domain and the partial C-domain and P-domain with the bilayer, particularly the coordination of the CRT P-domain, plays an important role for the more open conformation of CRT in the TSP1−CRT complex on a raftlike

dx.doi.org/10.1021/bi500662v | *Biochemistry* 2014, 53, 6309−6322

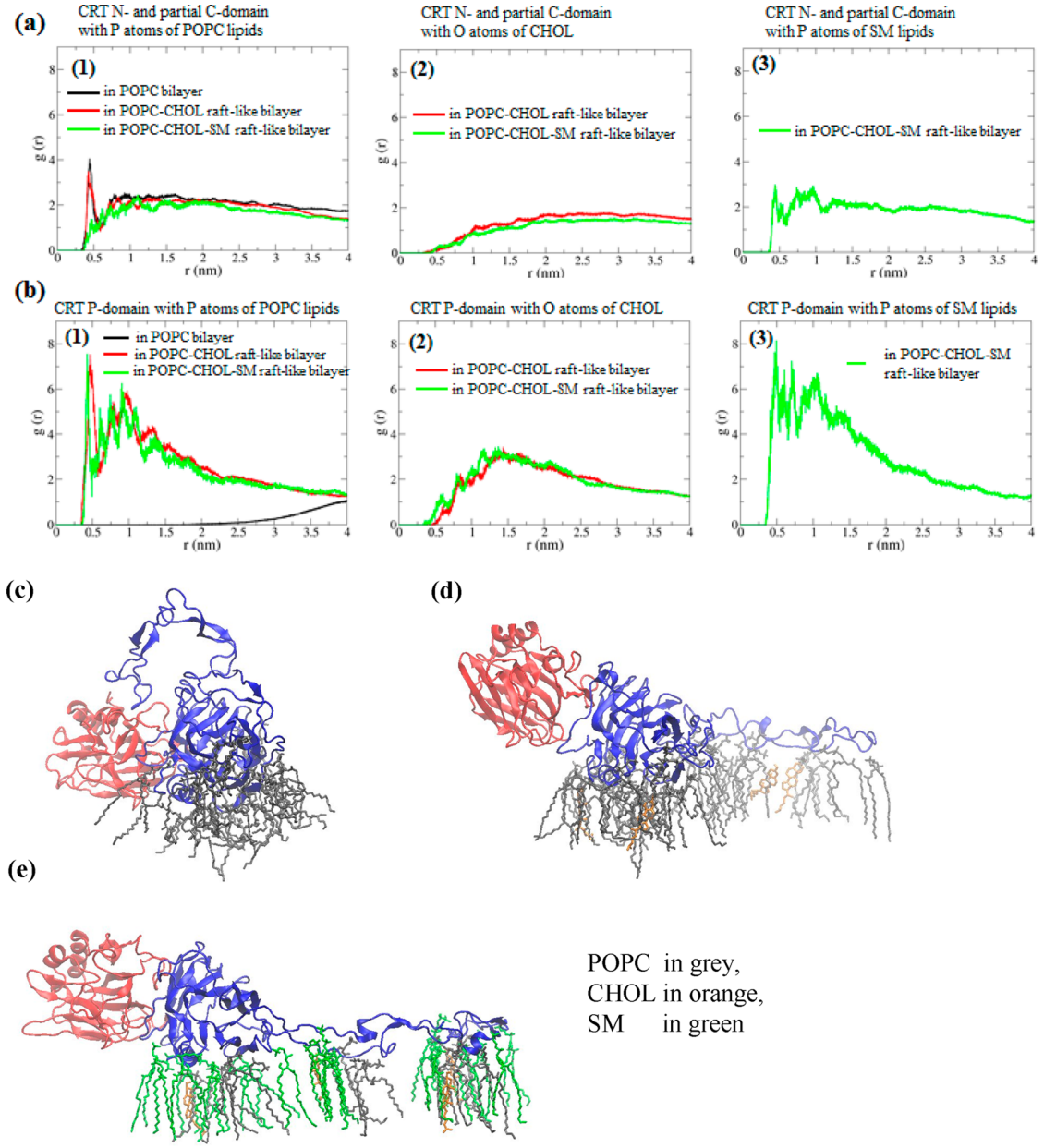

Figure 9. Comparison of the coordination of the N-domain and partial C- and P-domains of CRT in the TSP1−CRT complex with the POPC lipids, CHOL molecules, and SM lipids on a POPC bilayer, on a POPC−CHOL raftlike lipid bilayer, and on a POPC−CHOL−SM raftlike lipid bilayer. (a) Radial distribution functions (RDFs) with respect to the CRT N-domain and the partial C-domain for the phosphorus atoms of the POPC lipid headgroup (1), the cholesterol hydroxyl oxygens (2), and the phosphorus atoms of the SM lipid headgroup (3). (b) RDFs with respect to the CRT P-domain for the phosphorus atoms of the POPC lipid headgroup (1), the cholesterol hydroxyl oxygens (2), and the phosphorus atoms of the SM lipid headgroup (3). (c−e) Snapshots of the MD trajectory showing the coordination of the N-domain and partial C- and P-domains of CRT in the TSP1−CRT complex with POPC lipids in a POPC bilayer, with POPC lipids and CHOL molecules in a POPC−CHOL raftlike lipid bilayer, and with POPC lipids, CHOL molecules, and SM lipids in a POPC−CHOL−SM raftlike lipid bilayer, respectively. The lipids and CHOL molecules whose atoms are within 3.5 Å of CRT are shown with CRT in panels c−e. TSP1 is colored red and CRT blue; POPC lipids are colored gray, CHOL molecules orange, and SM lipids green.

lipid bilayer compared to that on a POPC bilayer as shown in Figures 5 and 6 and Figure S5 of the Supporting Information.

Analyses of the Effect of Cell Surface Protein CRT on Lipid or CHOL Molecule Coordination and Aggregation in a Raftlike Lipid Bilayer. The interactions of CRT or the TSP1−CRT complex with the lipid bilayer in different bilayer environments could also affect the coordination and/or aggregation of POPC lipids, CHOL molecules, and SM lipids to influence the raftlike bilayer structure that could in turn influence the CRT−bilayer interactions, CRT conformational changes, and TSP1−CRT interactions. We compared the RDFs among the POPC lipids, CHOL molecules, and SM lipids in a POPC−CHOL raftlike bilayer and a POPC−CHOL−SM raftlike bilayer with the CRT effect, with the TSP1−CRT complex effect, and without the protein's effect (Figure S6 of the Supporting Information). Results showed that for a POPC−CHOL raftlike lipid bilayer, with the CRT or the TSP1−CRT complex effects, cholesterol hydroxyl oxygens with cholesterol hydroxyl oxygens [Figure S6a (1) of the Supporting Information], cholesterol hydroxyl oxygens with the phospho-

dx.doi.org/10.1021/bi500662v | *Biochemistry* 2014, 53, 6309−6322

rus atoms of the POPC lipid headgroup [Figure S6a (2) of the Supporting Information], and the phosphorus atoms of the POPC lipid headgroup with the phosphorus atoms of the POPC lipid headgroup [Figure S6a (3) of the Supporting Information] were more coordinated compared to those without a protein effect on the bilayer. For a POPC−CHOL−SM raftlike lipid bilayer, with the CRT or the TSP1−CRT complex effects, hydroxyl oxygens with cholesterol hydroxyl oxygens [Figure S6b (1) of the Supporting Information], cholesterol hydroxyl oxygens with the phosphorus atoms of the SM lipid headgroup [Figure S6b (2) of the Supporting Information], cholesterol hydroxyl oxygens with the phosphorus atoms of the POPC lipid headgroup [Figure S6b (3) of the Supporting Information], phosphorus atoms of the SM lipid headgroup with the phosphorus atoms of the SM lipid headgroup [Figure S6b (4) of the Supporting Information], phosphorus atoms of the SM lipid headgroup with the phosphorus atoms of the POPC lipid headgroup [Figure S6b (5) of the Supporting Information], and phosphorus atoms of the POPC lipid headgroup with the phosphorus atoms of the POPC lipid headgroup [Figure S6b (6) of the Supporting Information] were more coordinated than those without a protein effect on the bilayer. These results indicated that the interaction of the CRT or the TSP1−CRT complex with the bilayer could cause the CHOL molecules and/or SM lipids to be more coordinated and to potentially aggregate into patchlike regions in the raftlike lipid bilayers.

CONCLUSION

We investigated the interactions of cell surface CRT, either alone or in a complex with TSP1, with a POPC bilayer, a POPC−CHOL raftlike lipid bilayer, and a POPC−CHOL−SM raftlike lipid bilayer via atomically detailed molecular dynamics simulations. Results showed that the microscopic structural properties of the lipid molecules and mesoscopic mechanical properties and electrostatic potential of the bilayer were significantly different between a POPC bilayer and a raftlike lipid bilayer and the difference was enhanced by SM lipids in a raftlike lipid bilayer. These differences in bilayer properties affect interactions of CRT with the bilayer, further affecting CRT conformation and TSP1−CRT interactions. A raftlike lipid bilayer environment stabilized CRT conformation and affected TSP1−CRT interactions compared to a POPC bilayer environment. Binding of TSP1 to CRT resulted in a more open conformation for the CRT N-domain with respect to the CRT P-domain in a raftlike lipid bilayer environment, which could facilitate binding of CRT to LRP1 to engage downstream signaling. The more open conformational changes of CRT by binding to TSP1 in a raftlike lipid bilayer environment were enhanced by SM lipids in a raftlike lipid bilayer. The direct interactions of the N-domain and partial C- and P-domains of CRT, particularly the P-domain of CRT, with the bilayer could contribute to the more open conformation of CRT in the TSP1−CRT complex on a raftlike lipid bilayer compared to that on a POPC bilayer. The interactions of CRT or the TSP1−CRT complex with the lipid bilayer also caused the CHOL molecules and/or lipids to be more coordinated to potentially aggregate into patchlike regions in the raftlike lipid bilayers. The coordination and aggregation of the lipid and CHOL molecule could in turn affect the interactions of CRT with the membrane raft, thereby altering TSP1−CRT interactions and CRT conformational changes that potentially regulate its interactions with LRP1. Results from this study provide molecular insights for the role of lipid bilayer environments on TSP1−CRT interactions and on the CRT conformational changes that potentially facilitate the binding of CRT to LRP1 to engage downstream signaling events.[10−15]

ASSOCIATED CONTENT

Supporting Information

List of residues in N- and P-domains of CRT in the interaction of the TSP1−CRT complex with the bilayer (Table S1), TSP1−CRT complex obtained from a previous study[45] (Figure S1), the simulation system for the TSP1−CRT complex on a POPC−CHOL raftlike lipid bilayer (Figure S2), equilibration of the simulated systems (Figure S3), the electrostatic potential of a POPC bilayer, a POPC−CHOL raftlike lipid bilayer, and a POPC−CHOL−SM raftlike lipid bilayer (Figure S4), a conformational comparison between the representative structures of TSP1-bound CRT and CRT alone on a POPC bilayer, on a POPC−CHOL raftlike lipid bilayer, and on a POPC−CHOL−SM raftlike lipid bilayer (Figure S5), and a comparison of the coordination among the POPC lipids, CHOL molecules, and SM lipids in a POPC−CHOL raftlike bilayer and a POPC−CHOL−SM raftlike lipid bilayer with a CRT effect, with a TSP1−CRT complex effect, and without the protein's effect (Figure S6). This material is available free of charge via the Internet at http://pubs.acs.org.

AUTHOR INFORMATION

Corresponding Author

*Department of Biomedical Engineering, The University of Alabama at Birmingham, 803 Shelby Interdisciplinary Biomedical Research Building, 1825 University Blvd., Birmingham, AL 35294. E-mail: yhsong@uab.edu. Phone: (205) 996-6939. Fax: (205) 975-4919.

Funding

This work was supported in part by an National Science Foundation (NSF) Grant CBET-1159859 to Y.S. and J.E.M.-U. and NSF Grant MCB-130026 to Y.S.

Notes

The authors declare no competing financial interest.

ACKNOWLEDGMENTS

We acknowledge computational resources from the Alabama Supercomputer Center and Supercomputer facility at The University of Alabama at Birmingham. We thank the anonymous reviewers for their helpful remarks.

REFERENCES

(1) Falanga, V. (2005) Wound healing and its impairment in the diabetic foot. *Lancet 366*, 1736−1743.

(2) Cheng, C. F., Fan, J., Fedesco, M., Guan, S., Li, Y., Bandyopadhyay, B., Bright, A. M., Yerushalmi, D., Liang, M., Chen, M., Han, Y. P., Woodley, D. T., and Li, W. (2008) Transforming growth factor α (TGFα)-stimulated secretion of HSP90α: Using the receptor LRP-1/CD91 to promote human skin cell migration against a TGFβ-rich environment during wound healing. *Mol. Cell. Biol. 28*, 3344−3358.

(3) Jung, M. Y., Thapa, N., Kim, J. E., Yang, J. D., Cho, B. C., and Kim, I. S. (2007) Recombinant tetra-cell adhesion motifs supports adhesion, migration and proliferation of keratinocytes/fibroblasts, and promotes wound healing. *Exp. Mol. Med. 39*, 663−672.

(4) Hara-Chikuma, M., and Verkman, A. S. (2008) Aquaporin-3 facilitates epidermal cell migration and proliferation during wound healing. *J. Mol. Med. 86*, 221−231.

(5) Rieck, P. W., Cholidis, S., and Hartmann, C. (2001) Intracellular signaling pathway of FGF-2-modulated corneal endothelial cell migration during wound healing in vitro. *Exp. Eye Res. 73*, 639−650.
(6) Ellis, I. R., and Schor, S. L. (1996) Differential effects of TGF-β1 on hyaluronan synthesis by fetal and adult skin fibroblasts: Implications for cell migration and wound healing. *Exp. Cell Res. 228*, 326−333.
(7) Grinnell, F. (1990) The activated keratinocyte: Up regulation of cell adhesion and migration during wound healing. *J. Trauma 30*, S144−S149.
(8) Seiler, W. O., Stahelin, H. B., Zolliker, R., Kallenberger, A., and Luscher, N. J. (1989) Impaired migration of epidermal cells from decubitus ulcers in cell cultures. A cause of protracted wound healing? *Am. J. Clin. Pathol. 92*, 430−434.
(9) Sweetwyne, M. T., Pallero, M. A., Lu, A., Van Duyn Graham, L., and Murphy-Ullrich, J. E. (2010) The calreticulin-binding sequence of thrombospondin 1 regulates collagen expression and organization during tissue remodeling. *Am. J. Pathol. 177*, 1710−1724.
(10) Pallero, M. A., Elzie, C. A., Chen, J., Mosher, D. F., and Murphy-Ullrich, J. E. (2008) Thrombospondin 1 binding to calreticulin-LRP1 signals resistance to anoikis. *FASEB J. 22*, 3968−3979.
(11) Barker, T. H., Pallero, M. A., MacEwen, M. W., Tilden, S. G., Woods, A., Murphy-Ullrich, J. E., and Hagood, J. S. (2004) Thrombospondin-1-induced focal adhesion disassembly in fibroblasts requires Thy-1 surface expression, lipid raft integrity, and Src activation. *J. Biol. Chem. 279*, 23510−23516.
(12) Orr, A. W., Pedraza, C. E., Pallero, M. A., Elzie, C. A., Goicoechea, S., Strickland, D. K., and Murphy-Ullrich, J. E. (2003) Low density lipoprotein receptor-related protein is a calreticulin coreceptor that signals focal adhesion disassembly. *J. Cell Biol. 161*, 1179−1189.
(13) Orr, A. W., Elzie, C. A., Kucik, D. F., and Murphy-Ullrich, J. E. (2003) Thrombospondin signaling through the calreticulin/LDL receptor-related protein co-complex stimulates random and directed cell migration. *J. Cell Sci. 116*, 2917−2927.
(14) Goicoechea, S., Pallero, M. A., Eggleton, P., Michalak, M., and Murphy-Ullrich, J. E. (2002) The anti-adhesive activity of thrombospondin is mediated by the N-terminal domain of cell surface calreticulin. *J. Biol. Chem. 277*, 37219−37228.
(15) Goicoechea, S., Orr, A. W., Pallero, M. A., Eggleton, P., and Murphy-Ullrich, J. E. (2000) Thrombospondin mediates focal adhesion disassembly through interactions with cell surface calreticulin. *J. Biol. Chem. 275*, 36358−36368.
(16) Li, S. S., Forslow, A., and Sundqvist, K. G. (2005) Autocrine regulation of T cell motility by calreticulin-thrombospondin-1 interaction. *J. Immunol. 174*, 654−661.
(17) Talme, T., Bergdahl, E., and Sundqvist, K. G. (2014) Regulation of T-lymphocyte motility, adhesion and de-adhesion by a cell surface mechanism directed by low density lipoprotein receptor-related protein 1 and endogenous thrombospondin-1. *Immunology 142*, 176−192.
(18) DiPietro, L. A., and Polverini, P. J. (1993) Angiogenic macrophages produce the angiogenic inhibitor thrombospondin 1. *Am. J. Pathol. 143*, 678−684.
(19) Reed, M. J., Iruela-Arispe, L., O'Brien, E. R., Truong, T., LaBell, T., Bornstein, P., and Sage, E. H. (1995) Expression of thrombospondins by endothelial cells. Injury is correlated with TSP-1. *Am. J. Pathol. 147*, 1068−1080.
(20) Majack, R. A., Cook, S. C., and Bornstein, P. (1986) Control of smooth muscle cell growth by components of the extracellular matrix: Autocrine role for thrombospondin. *Proc. Natl. Acad. Sci. U.S.A. 83*, 9050−9054.
(21) Frangogiannis, N. G., Ren, G., Dewald, O., Zymek, P., Haudek, S., Koerting, A., Winkelmann, K., Michael, L. H., Lawler, J., and Entman, M. L. (2005) Critical role of endogenous thrombospondin-1 in preventing expansion of healing myocardial infarcts. *Circulation 111*, 2935−2942.
(22) Bornstein, P. (2001) Thrombospondins as matricellular modulators of cell function. *J. Clin. Invest. 107*, 929−934.
(23) Mosher, D. F., Doyle, M. J., and Jaffe, E. A. (1982) Synthesis and secretion of thrombospondin by cultured human endothelial cells. *J. Cell Biol. 93*, 343−348.
(24) Lawler, J. W., Slayter, H. S., and Coligan, J. E. (1978) Isolation and characterization of a high molecular weight glycoprotein from human blood platelets. *J. Biol. Chem. 253*, 8609−8616.
(25) Jaffe, E. A., Ruggiero, J. T., Leung, L. K., Doyle, M. J., McKeown-Longo, P. J., and Mosher, D. F. (1983) Cultured human fibroblasts synthesize and secrete thrombospondin and incorporate it into extracellular matrix. *Proc. Natl. Acad. Sci. U.S.A. 80*, 998−1002.
(26) Jaffe, E. A., Ruggiero, J. T., and Falcone, D. J. (1985) Monocytes and macrophages synthesize and secrete thrombospondin. *Blood 65*, 79−84.
(27) Raugi, G. J., Mumby, S. M., Abbott-Brown, D., and Bornstein, P. (1982) Thrombospondin: Synthesis and secretion by cells in culture. *J. Cell Biol. 95*, 351−354.
(28) Adams, J. C., and Lawler, J. (2004) The thrombospondins. *Int. J. Biochem. Cell Biol. 36*, 961−968.
(29) Adams, J. C. (2001) Thrombospondins: Multifunctional regulators of cell interactions. *Annu. Rev. Cell Dev. Biol. 17*, 25−51.
(30) Sweetwyne, M. T., and Murphy-Ullrich, J. E. (2012) Thrombospondin1 in tissue repair and fibrosis: TGF-β-dependent and independent mechanisms. *Matrix Biol. 31*, 178−186.
(31) Li, S. S., Ivanoff, A., Bergstrom, S. E., Sandstrom, A., Christensson, B., van Nerven, J., Holgersson, J., Hauzenberger, D., Arencibia, I., and Sundqvist, K. G. (2002) T lymphocyte expression of thrombospondin-1 and adhesion to extracellular matrix components. *Eur. J. Immunol. 32*, 1069−1079.
(32) Li, S. S., Liu, Z., Uzunel, M., and Sundqvist, K. G. (2006) Endogenous thrombospondin-1 is a cell-surface ligand for regulation of integrin-dependent T-lymphocyte adhesion. *Blood 108*, 3112−3120.
(33) Murphy-Ullrich, J. E., Gurusiddappa, S., Frazier, W. A., and Hook, M. (1993) Heparin-binding peptides from thrombospondins 1 and 2 contain focal adhesion-labilizing activity. *J. Biol. Chem. 268*, 26784−26789.
(34) Tan, K., Duquette, M., Liu, J. H., Zhang, R., Joachimiak, A., Wang, J. H., and Lawler, J. (2006) The structures of the thrombospondin-1 N-terminal domain and its complex with a synthetic pentameric heparin. *Structure 14*, 33−42.
(35) Johnson, S., Michalak, M., Opas, M., and Eggleton, P. (2001) The ins and outs of calreticulin: From the ER lumen to the extracellular space. *Trends Cell Biol. 11*, 122−129.
(36) Ling, S., Pi, X., and Holoshitz, J. (2007) The rheumatoid arthritis shared epitope triggers innate immune signaling via cell surface calreticulin. *J. Immunol. 179*, 6359−6367.
(37) Gold, L. I., Eggleton, P., Sweetwyne, M. T., Van Duyn, L. B., Greives, M. R., Naylor, S. M., Michalak, M., and Murphy-Ullrich, J. E. (2010) Calreticulin: Non-endoplasmic reticulum functions in physiology and disease. *FASEB J. 24*, 665−683.
(38) Arosa, F. A., de Jesus, O., Carmo, A. M., Porto, G., and de Sousa, M. (1999) Calreticulin is expressed on the T cell surface of activated human peripheral blood T lymphocytes in association with MHC-class I molecules. *FASEB J. 13*, A274.
(39) Arosa, F. A., de Jesus, O., Porto, G., Carmo, A. M., and de Sousa, M. (1999) Calreticulin is expressed on the cell surface of activated human peripheral blood T lymphocytes in association with major histocompatibility complex class I molecules. *J. Biol. Chem. 274*, 16917−16922.
(40) Zimmerman, K. A., Graham, L. V., Pallero, M. A., and Murphy-Ullrich, J. E. (2013) Calreticulin regulates transforming growth factor-β-stimulated extracellular matrix production. *J. Biol. Chem. 288*, 14584−14598.
(41) Zhu, Q., Zelinka, P., White, T., and Tanzer, M. L. (1997) Calreticulin-integrin bidirectional signaling complex. *Biochem. Biophys. Res. Commun. 232*, 354−358.
(42) Kwon, M. S., Park, C. S., Choi, K., Ahnn, J., Kim, J. I., Eom, S. H., Kaufman, S. J., and Song, W. K. (2000) Calreticulin couples calcium release and calcium influx in integrin-mediated calcium signaling. *Mol. Biol. Cell 11*, 1433−1443.

(43) Gold, L. I., Rahman, M., Blechman, K. M., Greives, M. R., Churgin, S., Michaels, J., Callaghan, M. J., Cardwell, N. L., Pollins, A. C., Michalak, M., Siebert, J. W., Levine, J. P., Gurtner, G. C., Nanney, L. B., Galiano, R. D., and Cadacio, C. L. (2006) Overview of the role for calreticulin in the enhancement of wound healing through multiple biological effects. *J. Invest. Dermatol. Symp. Proc. 11*, 57−65.
(44) Norgaard, T. K., Larsen, N., Steen Jørgensen, F., Hojrup, P., Houen, G., and Vestergaard, B. (2008) Small angle X-ray scattering study of calreticulin reveals conformational plasticity. *Biochim. Biophys. Acta 1784*, 1265−1270.
(45) Yan, Q., Murphy-Ullrich, J. E., and Song, Y. H. (2010) Structural Insight into the Role of Thrombospondin-1 Binding to Calreticulin in Calreticulin-Induced Focal Adhesion Disassembly. *Biochemistry 49*, 3685−3694.
(46) Pike, L. J. (2006) Rafts defined: A report on the Keystone Symposium on Lipid Rafts and Cell Function. *J. Lipid Res. 47*, 1597−1598.
(47) Simons, K., and Ikonen, E. (1997) Functional rafts in cell membranes. *Nature 387*, 569−572.
(48) Ostrom, R. S., and Insel, P. A. (2004) The evolving role of lipid rafts and caveolae in G protein-coupled receptor signaling: Implications for molecular pharmacology. *Br. J. Pharmacol. 143*, 235−245.
(49) Maguy, A., Hebert, T. E., and Nattel, S. (2006) Involvement of lipid rafts and caveolae in cardiac ion channel function. *Cardiovasc. Res. 69*, 798−807.
(50) Barker, T. H., Pallero, M. A., MacEwen, M. W., Tilden, S. G., Woods, A., Murphy-Ullrich, J. E., and Hagood, J. S. (2004) Thrombospondin-1-induced focal adhesion disassembly in fibroblasts requires Thy-1 surface expression, lipid raft integrity, and Src activation. *J. Biol. Chem. 279*, 23510−23516.
(51) DeBruin, L. S., and Harauz, G. (2007) White matter rafting: Membrane microdomains in myelin. *Neurochem. Res. 32*, 213−228.
(52) Berkowitz, M. L. (2009) Detailed molecular dynamics simulations of model biological membranes containing cholesterol. *Biochim. Biophys. Acta 1788*, 86−96.
(53) Bennett, W. F. D., and Tieleman, D. P. (2013) Computer simulations of lipid membrane domains. *Biochim. Biophys. Acta 1828*, 1765−1776.
(54) Hess, B., Kutzner, C., van der Spoel, D., and Lindahl, E. (2008) GROMACS 4: Algorithms for highly efficient, load-balanced, and scalable molecular simulation. *J. Chem. Theory Comput 4*, 435−447.
(55) Kaiser, H. J., Lingwood, D., Levental, I., Sampaio, J. L., Kalvodova, L., Rajendran, L., and Simons, K. (2009) Order of lipid phases in model and plasma membranes. *Proc. Natl. Acad. Sci. U.S.A. 106*, 16645−16650.
(56) Epand, R. F., Sayer, B. G., and Epand, R. M. (2005) Induction of raft-like domains by a myristoylated NAP-22 peptide and its Tyr mutant. *FEBS J. 272*, 1792−1803.
(57) Bennett, W. F. D., and Tieleman, D. P. (2012) Molecular simulation of rapid translocation of cholesterol, diacylglycerol, and ceramide in model raft and nonraft membranes. *J. Lipid Res. 53*, 421−429.
(58) Crane, J. M., and Tamm, L. K. (2004) Role of cholesterol in the formation and nature of lipid rafts in planar and spherical model membranes. *Biophys. J. 86*, 2965−2979.
(59) McMullen, T. P. W., Lewis, R. N. A. H., and McElhaney, R. N. (2004) Cholesterol-phospholipid interactions, the liquid-ordered phase and lipid rafts in model and biological membranes. *Curr. Opin. Colloid Interface Sci. 8*, 459−468.
(60) Forrest, L. R., Tieleman, D. P., and Sansom, M. S. P. (1999) Defining the transmembrane helix of M2 protein from influenza A by molecular dynamics simulations in a lipid bilayer. *Biophys. J. 76*, 1886−1896.
(61) Law, R. J., Tieleman, D. P., and Sansom, M. S. P. (2003) Pores formed by the nicotinic receptor M2 delta peptide: A molecular dynamics simulation study. *Biophys. J. 84*, 14−27.
(62) Hub, J. S., Winkler, F. K., Merrick, M., and de Groot, B. L. (2010) Potentials of Mean Force and Permeabilities for Carbon Dioxide, Ammonia, and Water Flux across a Rhesus Protein Channel and Lipid Membranes. *J. Am. Chem. Soc. 132*, 13251−13263.
(63) Wennberg, C. L., van der Spoel, D., and Hub, J. S. (2012) Large Influence of Cholesterol on Solute Partitioning into Lipid Membranes. *J. Am. Chem. Soc. 134*, 5351−5361.
(64) Niemela, P. S., Ollila, S., Hyvonen, M. T., Karttunen, M., and Vattulainen, I. (2007) Assessing the nature of lipid raft membranes. *PLoS Comput. Biol. 3*, 304−312.
(65) Schrag, J. D., Bergeron, J. J., Li, Y., Borisova, S., Hahn, M., Thomas, D. Y., and Cygler, M. (2001) The Structure of calnexin, an ER chaperone involved in quality control of protein folding. *Mol. Cell 8*, 633−644.
(66) Ellgaard, L., Riek, R., Braun, D., Herrmann, T., Helenius, A., and Wuthrich, K. (2001) Three-dimensional structure topology of the calreticulin P-domain based on NMR assignment. *FEBS Lett. 488*, 69−73.
(67) Guo, L., Groenendyk, J., Papp, S., Dabrowska, M., Knoblach, B., Kay, C., Parker, J. M., Opas, M., and Michalak, M. (2003) Identification of an N-domain histidine essential for chaperone function in calreticulin. *J. Biol. Chem. 278*, 50645−50653.
(68) Humphrey, W., Dalke, A., and Schulten, K. (1996) VMD: Visual molecular dynamics. *J. Mol. Graphics Modell. 14*, 33−38.
(69) Berger, O., Edholm, O., and Jahnig, F. (1997) Molecular dynamics simulations of a fluid bilayer of dipalmitoylphosphatidylcholine at full hydration, constant pressure, and constant temperature. *Biophys. J. 72*, 2002−2013.
(70) Poger, D., and Mark, A. E. (2012) Lipid bilayers: The effect of force field on ordering and dynamics. *J. Chem. Theory Comput. 8*, 4807−4817.
(71) Scott, W. R. P., Hunenberger, P. H., Tironi, I. G., Mark, A. E., Billeter, S. R., Fennen, J., Torda, A. E., Huber, T., Kruger, P., and van Gunsteren, W. F. (1999) The GROMOS biomolecular simulation program package. *J. Phys. Chem. A 103*, 3596−3607.
(72) Berendsen, H. J. C., Postma, J. P. M., van Gunsteren, W. F., and Hermans, J. (1981) Interaction models for water in relation to protein hydration. In *Intermolecular Forces* (Pullman, B., Ed.) pp 331−342, Springer, Dordrecht, The Netherlands.
(73) Yan, Q., McDonald, J. M., Zhou, T., and Song, Y. (2013) Structural insight for the roles of fas death domain binding to FADD and oligomerization degree of the Fas-FADD complex in the death-inducing signaling complex formation: A computational study. *Proteins 81*, 377−385.
(74) Yan, Q., Murphy-Ullrich, J. E., and Song, Y. (2011) Molecular and structural insight into the role of key residues of thrombospondin-1 and calreticulin in thrombospondin-1-calreticulin binding. *Biochemistry 50*, 566−573.
(75) Pan, D., Yan, Q., Chen, Y., McDonald, J. M., and Song, Y. (2011) Trifluoperazine regulation of calmodulin binding to Fas: A computational study. *Proteins 79*, 2543−2556.
(76) Pan, D., and Song, Y. (2010) Role of altered sialylation of the I-like domain of β1 integrin in the binding of fibronectin to β1 integrin: Thermodynamics and conformational analyses. *Biophys. J. 99*, 208−217.
(77) Suever, J. D., Chen, Y., McDonald, J. M., and Song, Y. (2008) Conformation and free energy analyses of the complex of calcium-bound calmodulin and the Fas death domain. *Biophys. J. 95*, 5913−5921.
(78) Liu, Y., Pan, D., Bellis, S. L., and Song, Y. (2008) Effect of altered glycosylation on the structure of the I-like domain of β1 integrin: A molecular dynamics study. *Proteins 73*, 989−1000.
(79) Lee, S. J., Song, Y., and Baker, N. A. (2008) Molecular dynamics simulations of asymmetric NaCl and KCl solutions separated by phosphatidylcholine bilayers: Potential drops and structural changes induced by strong Na^+-lipid interactions and finite size effects. *Biophys. J. 94*, 3565−3576.
(80) Song, Y., Guallar, V., and Baker, N. A. (2005) Molecular dynamics simulations of salicylate effects on the micro- and mesoscopic properties of a dipalmitoylphosphatidylcholine bilayer. *Biochemistry 44*, 13425−13438.

(81) Hess, B., Bekker, H., Berendsen, H. J. C., and Fraaije, J. G. E. M. (1997) LINCS: A linear constraint solver for molecular simulations. *J. Comput. Chem. 18*, 1463−1472.
(82) Nose, S. (1984) A unified formulation of the constant temperature molecular-dynamics methods. *J. Chem. Phys. 81*, 511−519.
(83) Hoover, W. G. (1985) Canonical dynamics: Equilibrium phase-space distributions. *Phys. Rev. A 31*, 1695−1697.
(84) Parrinello, M., and Rahman, A. (1981) Polymorphic transitions in single crystals: A new molecular dynamics. *J. Appl. Phys. 52*, 7182−7190.
(85) de Almeida, R. F. M., Fedorov, A., and Prieto, M. (2003) Sphingomyelin/phosphatidylcholine/cholesterol phase diagram: Boundaries and composition of lipid rafts. *Biophys. J. 85*, 2406−2416.
(86) Darden, T., York, D., and Pedersen, L. (1993) Particle Mesh Ewald: An N.Log(N) Method for Ewald Sums in Large Systems. *J. Chem. Phys. 98*, 10089−10092.
(87) Essmann, U., Perera, L., Berkowitz, M. L., Darden, T., Lee, H., and Pedersen, L. G. (1995) A Smooth Particle Mesh Ewald Method. *J. Chem. Phys. 103*, 8577−8593.
(88) Allen, M. P., and Tildesley, D. J. (1987) *Computer Simulation of Liquids*, Oxford University Press, New York.
(89) Efron, B., and Tibshirani, R. J. (1998) *An Introduction to the Bootstrap*, Chapman & Hall, New York.
(90) Bailey, N. T. J. (1995) *Statistical methods in biology*, 3rd ed., Cambridge University Press, New York.
(91) Gurtovenko, A. A., and Vattulainen, I. (2008) Effect of NaCl and KCl on phosphatidylcholine and phosphatidylethanolamine lipid membranes: Insight from atomic-scale simulations for understanding salt-induced effects in the plasma membrane. *J. Phys. Chem. B 112*, 1953−1962.
(92) Hyslop, P. A., Morel, B., and Sauerheber, R. D. (1990) Organization and Interaction of Cholesterol and Phosphatidylcholine in Model Bilayer-Membranes. *Biochemistry 29*, 1025−1038.
(93) Kucerka, N., Tristram-Nagle, S., and Nagle, J. F. (2005) Structure of fully hydrated fluid phase lipid bilayers with monounsaturated chains. *J. Membr. Biol. 208*, 193−202.
(94) Lantzsch, G., Binder, H., Heerklotz, H., Wendling, M., and Klose, G. (1996) Surface areas and packing constraints in POPC/$C_{12}EO_n$ membranes. A time-resolved fluorescence study. *Biophys. Chem. 58*, 289−302.
(95) Smaby, J. M., Momsen, M. M., Brockman, H. L., and Brown, R. E. (1997) Phosphatidylcholine acyl unsaturation modulates the decrease in interfacial elasticity induced by cholesterol. *Biophys. J. 73*, 1492−1505.
(96) Egberts, E., and Berendsen, H. J. C. (1988) Molecular-dynamics simulation of a smectic liquid crystal with atomic detail. *J. Chem. Phys. 89*, 3718−3732.
(97) Roux, B., and Schulten, K. (2004) Computational studies of membrane channels. *Structure 12*, 1343−1351.
(98) Feller, S. E., and Pastor, R. W. (1999) Constant surface tension simulations of lipid bilayers: The sensitivity of surface areas and compressibilities. *J. Chem. Phys. 111*, 1281−1287.
(99) Lindahl, E., and Edholm, O. (2000) Mesoscopic undulations and thickness fluctuations in lipid bilayers from molecular dynamics simulations. *Biophys. J. 79*, 426−433.
(100) Lingwood, D., and Simons, K. (2010) Lipid Rafts As a Membrane-Organizing Principle. *Science 327*, 46−50.
(101) Vereb, G., Szollosi, J., Matko, J., Nagy, P., Farkas, T., Vigh, L., Matyus, L., Waldmann, T. A., and Damjanovich, S. (2003) Dynamic, yet structured: The cell membrane three decades after the Singer-Nicolson model. *Proc. Natl. Acad. Sci. U.S.A. 100*, 8053−8058.
(102) Korade, Z., and Kenworthy, A. K. (2008) Lipid rafts, cholesterol, and the brain. *Neuropharmacology 55*, 1265−1273.
(103) Simons, K., and Ehehalt, R. (2002) Cholesterol, lipid rafts, and disease. *J. Clin. Invest. 110*, 597−603.
(104) London, E. (2002) Insights into lipid raft structure and formation from experiments in model membranes. *Curr. Opin. Struct. Biol. 12*, 480−486.
(105) Dupree, J. L., and Pomicter, A. D. (2010) Myelin, DIGs, and membrane rafts in the central nervous system. *Prostaglandins Other Lipid Mediators 91*, 118−129.
(106) Samsonov, A. V., Mihalyov, I., and Cohen, F. S. (2001) Characterization of cholesterol-sphingomyelin domains and their dynamics in bilayer membranes. *Biophys. J. 81*, 1486−1500.
(107) Kucerka, N., Perlmutter, J. D., Pan, J., Tristram-Nagle, S., Katsaras, J., and Sachs, J. N. (2008) The effect of cholesterol on short- and long-chain monounsaturated lipid bilayers as determined by molecular dynamics simulations and X-ray scattering. *Biophys. J. 95*, 2792−2805.
(108) Huang, J. Y., and Feigenson, G. W. (1999) A microscopic interaction model of maximum solubility of cholesterol in lipid bilayers. *Biophys. J. 76*, 2142−2157.
(109) Feig, M., Karanicolas, J., and Brooks, C. L. I. (2004) MMTSB Tool Set: Enhanced sampling and multiscale modeling methods for applications in structural biology. *J. Mol. Graphics Modell. 22*, 377−395.
(110) Hartigan, J. A. (1975) *Clustering algorithms*, John Wiley & Sons, Inc., New York.
(111) Herz, J., and Strickland, D. K. (2001) LRP: A multifunctional scavenger and signaling receptor. *J. Clin. Invest. 108*, 779−784.